Reactions of Fe-Cr and Ni-Cr Alloys in CO/CO_2 Gases at 850 and 950 °C

JEFFERY A. COLWELL and ROBERT A. RAPP

A series of Fe-Cr and Ni-Cr solid solution alloys was reacted at 850 and 950 °C in CO/CO_2 gas mixtures in which FeO and NiO were unstable. The competitive tendencies toward the carburization and oxidation of the chromium solute, as compared to a graphical thermodynamic "metastability" criterion, were tested experimentally. Relatively good agreement was found between predictions and experiments for the occurrence of Cr carburization beneath Cr_2O_3 internal oxides or external scales. The chromium contents required for the transition from internal oxidation of Cr to the formation of Cr_2O_3 external scales in CO/CO_2 gas mixtures were established for Fe-Cr and Ni-Cr alloys. The Cr_2O_3 external scales formed on Fe-Cr alloys were found to be relatively impervious to carbon penetration for short (12-hour) experiments. No carburization was observed in the Ni-Cr alloys, but the only alloys that were predicted to carburize were the ones that formed external scales.

I. INTRODUCTION

In coal conversion systems and other industrial environments, engineering alloys come into contact with several potential gaseous oxidants at relatively low oxygen potentials and high temperatures. Oxygen, sulfur, carbon, and nitrogen in the environment may participate in scale formation, or alternatively, reactions can occur internally by precipitation of product phases within grains or along grain boundaries. In either case, it is important to manipulate either the alloy composition or the environment to minimize these tendencies.

Upon the reaction of an alloy with multiple gaseous oxidants at high temperatures, any prediction of corrosion morphology or of the kinetics of reaction is difficult. For an alloy protected from oxidation by an adherent oxide scale, the maintenance of the scale requires the availability of the protective component at the alloy/oxide interface. For example, protective Cr_2O_3 scales on Fe-Cr alloys require Cr diffusion in the alloy to the alloy/scale interface to replace Cr atoms lost to oxidation. However, if a second oxidant such as sulfur or carbon can diffuse into the alloy to form chromium sulfides or carbides, the availability of chromium for scale growth is decreased and breakdown of the oxide scale becomes possible. Obviously, the competition between sulfur, oxygen, and carbon in a relatively reducing gas phase for reaction with chromium in the alloy will determine the corrosion morphology and kinetics.

Previous studies of internal precipitation reactions have dealt mostly with the reactions of alloys in gases containing only a single oxidant. Few investigations have been carried out in two-oxidant gases where a single alloy component can form two different compounds in the alloy. However, Hopkinson and Copson[1] have investigated the reaction of alloys in two-oxidant gases. They reported that nickel-chromium base alloys formed both internal oxides and carbides in CO/CO_2 mixtures. Also, Pettit, Goebel, and Goward[2] have studied alloy reactions in mixed gases and presented a theoretical treatment of the stability of product phases.

In this investigation, rather than studying the reaction of commercial alloys containing many alloying elements in multiple oxidants at high temperatures, a more simplified (model) approach was chosen in an attempt to understand the basic mechanism involved. In particular, two sets of binary alloy compositions where reacted in a two-oxidant gas. Iron-chromium and nickel-chromium alloys were chosen since these form the basis for many high-temperature alloys. Reactions in CO/CO_2 gas mixtures were studied since equilibrium oxygen and carbon activities can be simultaneously established. Alloys ranging from dilute to concentrated were tested to determine any influence of the second oxidant on the transition from internal oxidation to external scaling. Because dilute alloys have insufficient chromium to form a continuous external scale, but rather form internal oxide precipitates, they should also be subject to the simultaneous precipitation of chromium carbide if the carbon activity of the environment exceeds some critical value for a given alloy composition. An important goal of this research was the testing of a thermodynamic criterion for the simultaneous formation of corrosion products involving a second oxidant — in this case carbon. By studying a range of compositions where dilute alloys would internally oxidize while concentrated alloys formed external scales, observations were made to decide whether the oxide scale was a barrier to carbon penetration, and, therefore, to internal carburization.

II. THERMODYNAMIC CONSIDERATIONS

Graphical thermodynamic predictions of corrosion product formation are made using phase stability plots. In this investigation, all CO/CO_2 gas mixtures were set so that iron or nickel remained noble relative to wustite or NiO formation. Thus, only phase stabilities in the Cr-C-O system need be considered because Cr was the only component in the binary alloy that could form a binary oxide or carbide. Even though the combinations of gas and alloy compositions in the Fe-Cr system were suitable to stabilize the ternary spinel $FeCr_2O_4$, this complication did not require any important change from the format just described because the spinel was observed only in the most dilute alloys.

JEFFERY A. COLWELL, formerly Graduate Student, The Ohio State University, is Principal Research Scientist, Battelle Columbus Division, Columbus, OH 43201. ROBERT A. RAPP is Professor, Department of Metallurgical Engineering, The Ohio State University, Columbus, OH 43210.

Manuscript submitted July 19, 1985.

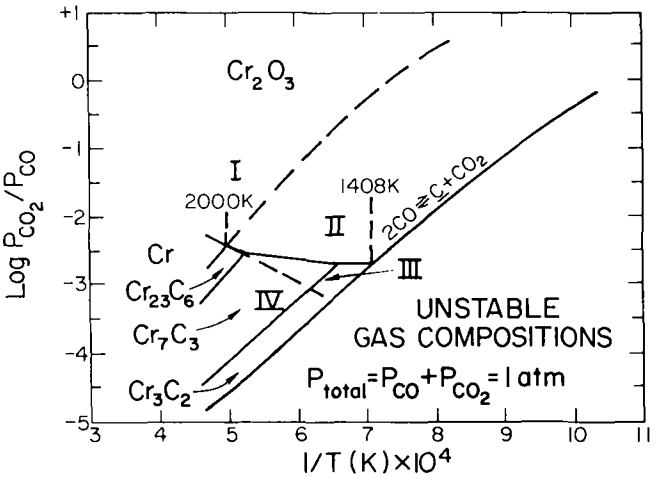

Fig. 1—Cr-C-O phase stability plot for pure Cr in CO/CO_2 gases.

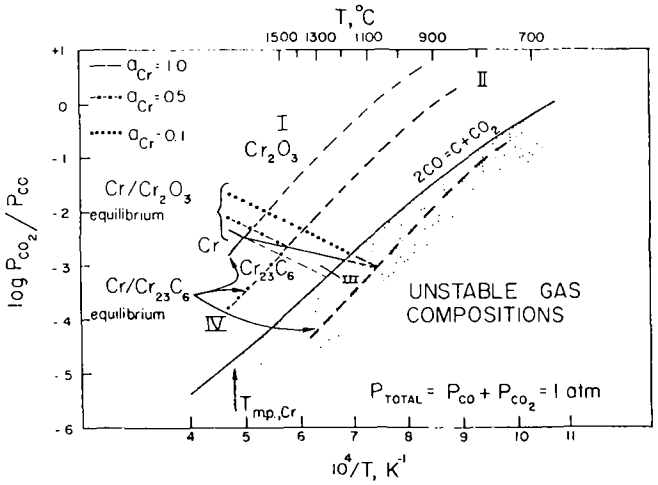

Fig. 2—Cr-C-O phase stability plot for Cr-containing alloys in CO/CO_2 gases. Shows the stable metal field expanding with decreasing chromium activity.

Figure 1 shows the phase stability regions in the Cr-C-O system, plotted as the logarithm of the CO_2/CO ratio *vs* reciprocal temperature. This diagram is calculated strictly from values for the standard Gibbs energies of formation for the binary compounds involved. The standard Gibbs energies of formation of the chromium carbides were taken from Kulkarni and Worrell;[3] the uncertainties in these values are as much as 5000 joules per mole of carbide for $Cr_{23}C_6$. Four zones (I, II, III, and IV) are shown on Figure 1. These zones are constructed by first extrapolating lines for metastable equilibria into stable phase fields. Zone I is the region bounded by the Cr/Cr_2O_3 stable equilibrium and the $Cr/Cr_{23}C_6$ metastable equilibrium where Cr_2O_3 is stable and the carbon activity is too low for metastable $Cr_{23}C_6$ formation. Zone II is bounded by the extrapolated $Cr/Cr_{23}C_6$ metastable equilibrium, the stable carbide/Cr_2O_3 equilibrium lines, and the Boudouard reaction line. (Gas mixtures to the right of the Boudouard reaction are unstable and decompose to form solid carbon.) In Zone II, although Cr_2O_3 is the equilibrium phase, the carbon activity is sufficiently high that $Cr_{23}C_6$ (or another carbide depending upon the gas mixture and temperature) is stable relative to pure Cr.

Zone III, the region bounded by the carbide/Cr_2O_3 equilibrium, the Cr/Cr_2O_3 metastable equilibrium, and the Boudouard reaction, represents thermodynamic stability for the chromium carbides and metastability for Cr_2O_3 relative to $Cr_{23}C_6$. Zone IV, the region bounded by the Cr/Cr_2O_3 metastable equilibrium, the Boudouard reaction, and the $Cr/Cr_{23}C_6$ equilibrium, corresponds to stable carbides only.

Figure 1 was calculated for pure Cr of unit activity and thus will not apply exactly in the case of an alloy containing chromium at a reduced activity. As chromium is alloyed with iron or nickel, the thermodynamic activity of Cr decreases and the stable metal field expands. Then the regions of Zones II and III decrease, as shown in Figure 2, where only the lowest carbide of chromium ($Cr_{23}C_6$) is considered for clarity. The Zone I/Zone II boundary is shown by the dashed lines. As the chromium activity is lowered, this boundary shifts to the right. This stability diagram predicts that in a Zone II gas of a given carbon activity, there is a critical chromium activity below which (metastable) carburization is thermodynamically impossible. For gases of the Boudouard composition, the critical Cr activities of Figure 2 lie between 0.1 and 0.5 depending upon temperature, and represent the intersection of the Zone I/Zone II boundary with the Boudouard line. This boundary does not have the same slope as the Boudouard line; thus, the critical chromium activity for carburization in a carbon-saturated gas will vary with temperature. Obviously the possibility of metastable (Zone II) $Cr_{23}C_6$ formation for any alloy at temperatures from 700 to 1100 °C will depend critically on the chromium activity in the alloy. Previous calculations of stable and metastable corrosion products have been made by Pettit, Goebel, and Goward,[2] but their results were not extended to a graphical interpretation.

Isothermal phase stability diagrams can also be constructed in which the carbon activity is plotted *vs* the oxygen activity. Figure 3 shows a schematic Cr-C-O stability plot. A solid horizontal line represents an alloy/carbide equilibrium, while a solid vertical line represents an alloy/oxide equilibrium. The same four zones that were defined in Figures 1 and 2 are also shown in Figure 3. Zone I is to the right of the alloy/oxide equilibrium boundary (in the stable Cr_2O_3 field) and below the metastable extension of the alloy/carbide boundary. Zone II (Cr_2O_3 stability, Cr-carbide metastability) is in the stable Cr_2O_3 field but above the metastable extension of the particular alloy/carbide boundary. The other two zones can be similarly defined.

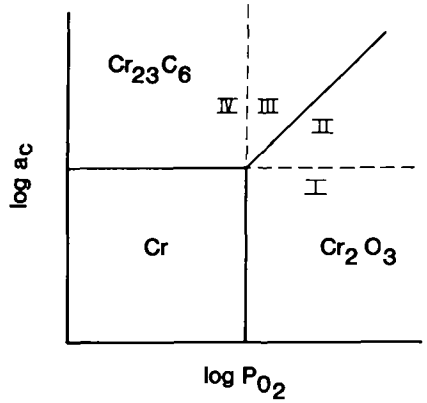

Fig. 3—Schematic isothermal phase stability diagram showing the four zones defined in Fig. 1.

Phase stability diagrams similar to Figure 3 were constructed for each alloy and temperature of this investigation. The activity of chromium for each Fe-Cr and Ni-Cr alloy at 950 and 850 °C was interpolated from activity data available from Mazandarany and Pehlke.[4] These chromium activities are listed in Table I. Figure 4 shows seven superimposed Fe-Cr-C-O phase stability plots, one for each alloy studied. The same four zones shown in Figure 3 can be constructed for each particular alloy. A line of constant total pressure of one atmosphere is also shown in the upper-right corner of Figure 4. For experiments at $P_{total} = 1$ atm, the oxygen activity and carbon activity cannot be varied independently but must change along the line of constant total pressure. The numbers on the line correspond to the experimental runs listed in Table II. Note that the oxygen partial pressures in all experimental gas mixtures are below the Fe-Fe_xO equilibrium. Consequently, iron should remain noble with respect to wustite formation in all experiments. In fact, for most of the alloys in this investigation, the lowest carbide, $Cr_{23}C_6$, is theoretically metastable with respect to Cr_7C_3 which is supposed to be the stable carbide. However, the spinel $FeCr_2O_4$ was stable (although usually not observed) for Fe-Cr alloys in all CO/CO_2 mixtures. It should be emphasized that Figure 4 is a calculated *equilibrium* phase stability diagram in which the lowest carbide is not always in equilibrium with the alloy. In the most dilute alloys, Cr_3C_2, the highest carbide, can be in equilibrium with the gas. An experimental study by Wada, Wada, Elliott, and Chipman[5] has described the equilibrium carbide stabilities for Fe-Cr alloys.

Table I. Chromium Activities for the Alloys Used in This Investigation

Alloy	a_{Cr} 850 °C	a_{Cr} 950 °C
Fe- 2.0 wt pct Cr	0.088	0.078
Fe- 4.9 wt pct Cr	0.16	0.14
Fe- 9.9 wt pct Cr	0.26	0.23
Fe-11.8 wt pct Cr	0.30	0.26
Fe-14.7 wt pct Cr	0.35	0.30
Fe-19.4 wt pct Cr	0.43	0.38
Fe-24.4 wt pct Cr	0.51	0.44
Ni- 1 wt pct Cr	0.0057	0.0056
Ni- 5 wt pct Cr	0.034	0.032
Ni- 6.75 wt pct Cr	0.050	0.047
Ni-10 wt pct Cr	0.084	0.079
Ni-15 wt pct Cr	0.15	0.14
Ni-21.4 wt pct Cr	0.31	0.28

From Figure 4 one can predict which alloys might form carbides in a given CO/CO_2 gas mixture according to a metastability criterion (Zone II gas:Cr_2O_3 stable, carbide metastable), and which ones should not. For example, consider the gas mixture used in experiment number 2 (shown on the $P_{total} = 1$ atm curve). If one extrapolates from point 2 of Figure 4 horizontally to the left, into the stable carbide fields, this particular carbon activity enters the stable carbide fields for the Fe-9.9, 11.8, 14.7, 19.4, and 24.4 wt pct Cr alloys, but the alloy fields are stable for the Fe-2.0 and 4.9 wt pct Cr alloys. Thus, in this Zone II gas of composition 2, Cr_2O_3 is stable in contact with the gas. For all alloys except Fe-2.0 and 4.9 pct Cr, chromium carbide (Cr_7C_3), although metastable relative to Cr_2O_3 for the alloy in contact with the gas phase, can become stable inside the alloy where the oxygen activity is lower than the equilibrium oxygen activity between Cr in the alloy and Cr_2O_3. These higher-Cr alloys would be expected to precipitate Cr_7C_3 beneath Cr_2O_3 if the surface could equilibrate to the carbon activity of the gas phase, and if carbon could diffuse into the alloy. Because the carbon activity in the alloy at a carbide precipitation front would be necessarily lower than that in the bulk gas, and because the dissolution of some iron into the carbide may affect the relative stabilities and nucleation rates of the various Cr carbides, the most stable pure carbide predicted might not be the one nucleated and grown

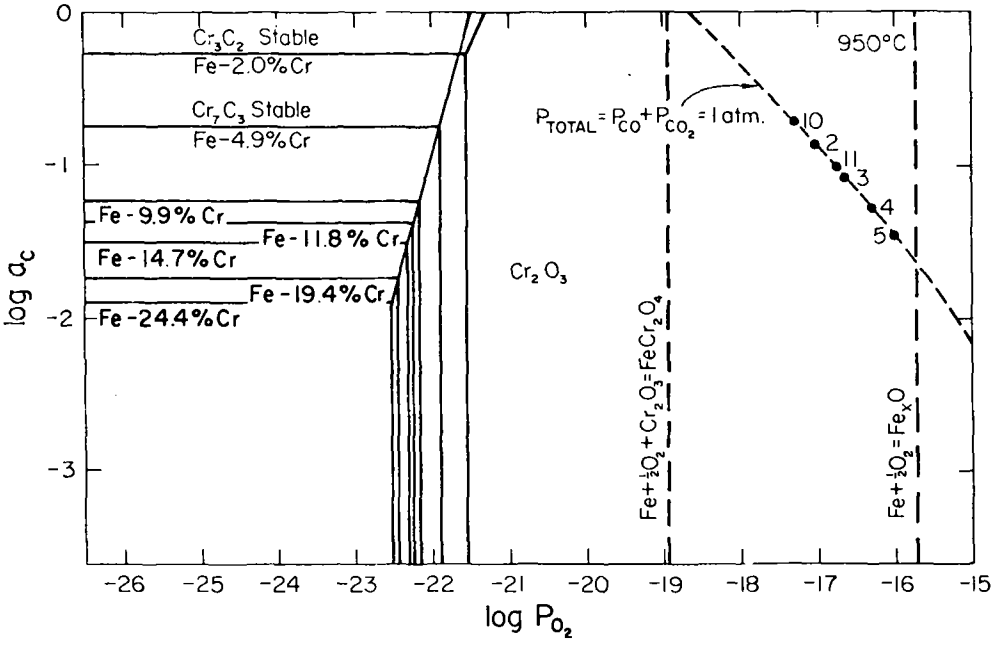

Fig. 4—Fe-Cr-C-O phase stability plot at 950 °C.

Table II. Specific Experimental Conditions

Expt.	CO_2/CO	Temp. (°C)	a_C	P_{O_2}	Time, Hours
2, Fe-Cr	0.11	950	0.136	9.62×10^{-18}	12
3, Fe-Cr	0.17	950	0.084	2.30×10^{-17}	12
4, Fe-Cr	0.25	950	0.053	4.97×10^{-17}	12
5, Fe-Cr	0.35	950	0.035	9.74×10^{-17}	12
6, Fe-Cr	0.31	850	0.175	5.65×10^{-19}	12
7, Fe-Cr	0.48	850	0.100	1.35×10^{-18}	12
8, Ni-Cr	0.70	850	0.060	2.88×10^{-18}	12
9, Ni-Cr	0.31	850	0.175	5.65×19^{-19}	12
10, both	0.08	950	0.193	5.09×10^{-18}	12
11, both	0.15	950	0.096	1.79×10^{-17}	12

at an internal carbide precipitation front. Further, the stable Cr_2O_3 may form either as an external scale or as internal oxide precipitates. While an external Cr_2O_3 scale may block inward carbon diffusion, Cr_2O_3 internal precipitates should permit carbon diffusion into the alloy matrix and carbide precipitation deeper in the alloy.

A graphical thermodynamic criterion for simultaneous carburization-oxidation of chromium-containing alloys in carbon- and oxygen-containing gases is proposed based on the above discussion. Experiments were conducted to test this hypothesis. Sets of Fe-Cr and Ni-Cr alloys of varying chromium activity were selected for reaction in the Zone II region of Figures 2 through 4. Furthermore, the gas mixtures were always selected so that Fe or Ni remained noble with respect to the formation of a binary Fe or Ni oxide. Thus, the transition from internal oxidation of Cr to external scaling in a two-oxidant gas could be studied without the complicating factor of binary Fe or Ni oxide products on the alloy surface.

III. EXPERIMENTAL PROCEDURE

The compositions, in weight percent, of the Fe-Cr and Ni-Cr alloys reacted in CO/CO_2 gases were as follows: Fe-2.0, 4.9, 9.9, 11.8, 14.7, 19.4, and 24.4Cr and Ni-1, 5, 6.75, 10, 15, and 21.4Cr. The Fe-Cr alloys were cast from high-purity components specifically for this investigation and a related study at Lockheed Palo Alto Research Labs.[6] Alloy plates were received in the hot-rolled condition. The Ni-Cr alloys were donated by Pratt and Whitney Aircraft and Battelle-Columbus Labs. The Ni-21.4Cr alloy was received as cold-rolled sheet and the other Ni-Cr alloys were received in the as-cast (chill block) condition.

Carbon monoxide of commercial purity (99.5 pct) was further purified by first passing over copper turnings at 400 °C, then over Ascarite to remove CO_2, and finally over magnesium perchlorate to remove water vapor. The copper turnings served a dual purpose: to remove oxygen, and to act as a hot surface where iron carbonyl could decompose. Prior to using this procedure, excessive sooting in the gas inlet tube and the exit line caused plugging and changes in the preset flowmeter setting due to an increase in back-pressure. Apparently, a reaction in the steel cylinder containing the CO gas formed iron carbonyl which later decomposed in the gas inlet tube into Fe and CO. The decomposed Fe then catalyzed the Boudouard reaction at low temperatures which caused sooting. Orange deposits found on the inside of the reaction tube were probably iron oxide. Passing carbon monoxide over the warm copper turnings minimized the sooting problem.

The carbon dioxide was dried by passing over magnesium perchlorate. The two gases were mixed in a chamber containing glass beads after passing through separate calibrated capillary flowmeters. The ratio of the flow rates established the partial pressure ratio.

A schematic diagram of the experimental apparatus is shown in Figure 5. A stabilized-zirconia electrolyte oxygen gauge was used to measure the CO_2/CO ratio in the reaction zone. The closed-end tube of ZrO_2-8 wt pct Y_2O_3 was platinized on the inside and outside surfaces of its tip and these electrodes were connected to Pt leadwires. At the reaction temperature, a voltage E was established between the electrodes according to

$$E = E^\circ - \frac{RT}{4F} \ln \frac{(P_{CO_2}/P_{CO})^2}{0.21} \quad [1]$$

where E° equals $(+\Delta G^\circ/4F)$ for the reaction

$$2CO_2 \rightleftharpoons 2CO + O_2 \quad [2]$$

For the air reference electrode ($P_{O_2} = 0.21$ atm), E° is 0.960 V at 850 °C and 0.916 V at 950 °C.

Samples prepared by successive grinding on 240, 320, 400, and 600 grit SiC papers were rinsed in acetone and dried by an air blast. All samples received a 2-hour anneal prior to reaction in the CO/CO_2 gas. Except for run 2 (where an Ar anneal was used), samples were annealed in flowing hydrogen, which caused no observable oxidation of chromium.

For a particular experiment, the gas mixture was set by adjusting the flowmeters. After the mixture was stable and the zirconia cell voltage constant, the samples were lowered into the furnace hot zone for 12 hours. All compositions were run for most of the experiments. The flowmeters were adjusted slightly throughout the experiment to maintain the desired voltage reading (±1 mV) from the zirconia cell. After 12 hours, the samples were raised from the hot zone in the CO/CO_2 gas mixture. After the samples were cool, the system was flushed with argon and the samples removed. All experimental conditions are summarized in Table II.

IV. RESULTS AND DISCUSSION

A selective etching technique described by Woodyatt and Krauss[7] was used to identify carbides. A potassium per-

manganate etch (4 g $KMnO_4$ + 4 g NaOH + 100 ml H_2O) stains $M_{23}C_6$ carbides tan while leaving M_7C_3 carbides unattacked. In all experiments, only $M_{23}C_6$ carbides were formed. From an experiment which produced carbides that etched tan, the alloy was dissolved in a methanol-10 pct Br solution; the residue was filtered and examined by X-ray diffraction. The only carbide present was $M_{23}C_6$. Also, the only carbides that were visible by using polarized light were the ones that etched tan. However, the staining etch gave better contrast than the polarized light technique.

In all of the alloys that carburized, the carbide formed was not the equilibrium M_7C_3 or M_3C_2 but the metastable $M_{23}C_6$. Consequently, the equilibrium phase stability diagrams (*e.g.*, Figure 4) were not applicable for predicting carburization during these experiments. Therefore, metastable Cr(Fe or Ni)-$Cr_{23}C_6$-Cr_2O_3 phase stability diagrams (*e.g.*, Figures 6 through 9) were developed to explain and predict $M_{23}C_6$ formation. The method of prediction from extrapolation of the carbon activity of a certain experiment into the carbide or alloy field for a particular alloy is the same as for the equilibrium diagrams. However, for a given alloy, the carburization prediction from the metastable diagram occurs at a higher carbon activity compared with the equilibrium diagrams, since the solubility of any metastable phase in a matrix is greater than that of a stable phase.

Indeed, the formation of $M_{23}C_6$ in the alloy represents a "double" metastability, since Cr_2O_3 is the stable phase formed from the alloy in contact with the gas phase, and Cr_7C_3 and Cr_3C_2 are generally the stable carbides in the alloy beneath a Cr_2O_3 layer. The metastable $M_{23}C_6$ carbide probably formed because of solution effects. Also, the metastable carbide $M_{23}C_6$ is cubic (as is the alloy matrix), but the equilibrium carbide M_7C_3 is trigonal. Thus, by the dissolution of some Fe into $M_{23}C_6$, the carbide stability can be increased, and because of its structure, it may be more readily nucleated.

Some representative photomicrographs which show the transition from internal oxidation to external scaling and the onset of carburization in Fe-Cr alloys are shown in Figures 10 through 14. All of these morphologies resulted from experiment 2 (see Table II). In Figure 10, no carburization was observed in the Fe-4.9 Cr alloy which internally oxidized. In Figure 11, the transition from internal oxidation to external scaling had not yet occurred for the Fe-9.9 Cr alloy but carburization had taken place. Carbides are found at the grain boundaries throughout the entire

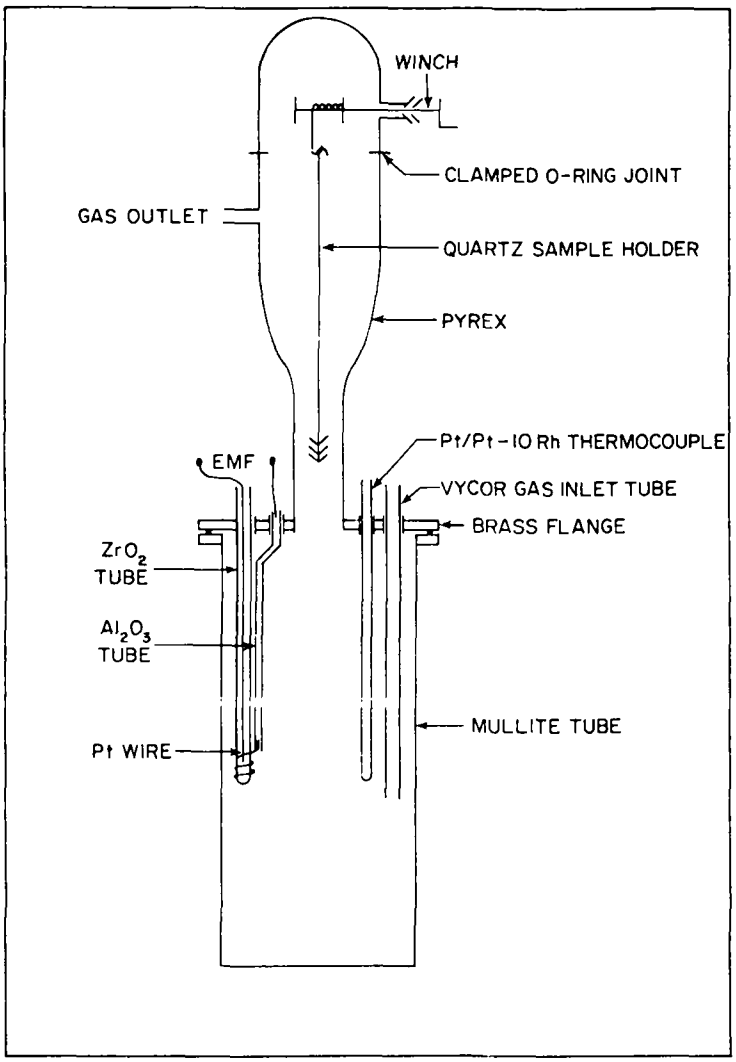

Fig. 5—Schematic representation of the experimental setup.

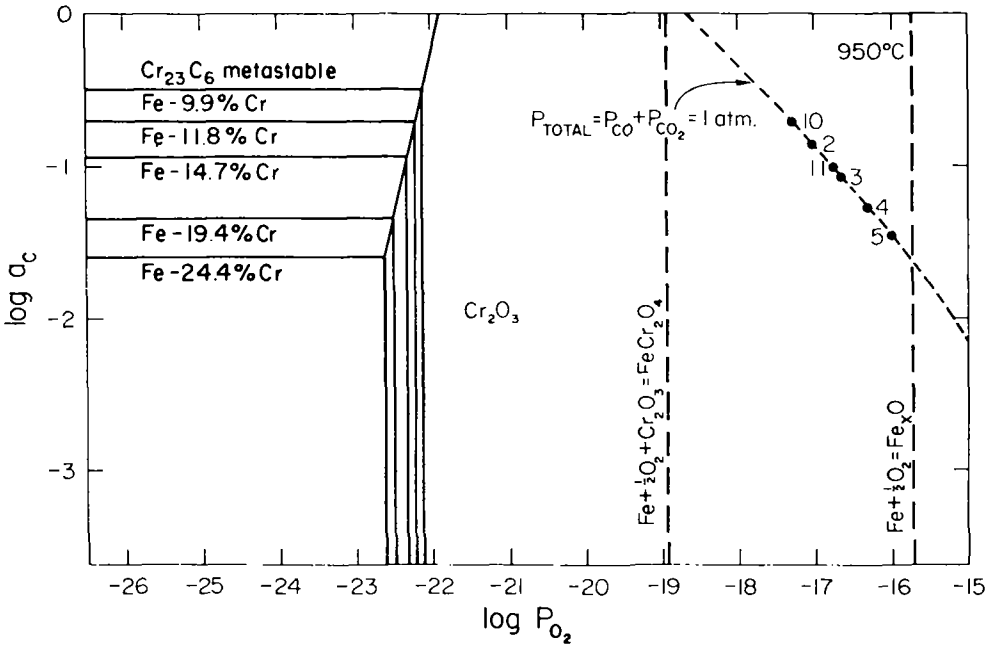

Fig. 6—Fe-Cr-C-O metastability plot at 950 °C.

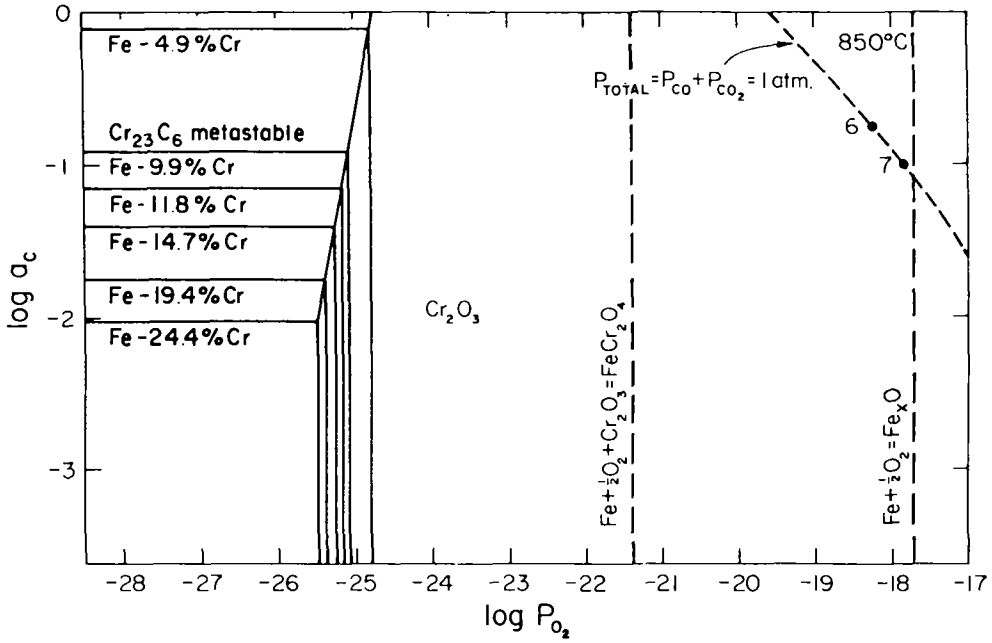

Fig. 7—Fe-Cr-C-O metastability plot at 850 °C.

cross-section. In fact, carburization for the Fe-9.9 Cr alloy in experiment 2 was not predicted, and the $M_{23}C_6$ must have been stabilized by the solution effect.

In Figure 12, carbon diffusion into the Fe-14.7 Cr alloy has stabilized the γ-phase at the surface in this originally ferritic alloy. The center of the sample is a two-phase $\alpha + \gamma$ structure. Carbide formation is observed only in the austenite zone near the alloy surface and has not yet proceeded into the two-phase region. This is consistent with the Fe-Cr-C sections published by Bungardt, Kunze, and Horn.[8] The austenite which was present at the reaction temperature was probably transformed to martensite during cooling as reported by Fujii and Meussner.[9] They reacted an Fe-15 Cr alloy at 900 °C in CO_2 and found the same type of microstructure as in this study. The carbon gradient through the alloy gives rise to the different regions in the cross-section. Figure 13 shows a higher magnification view of the same alloy. Internal films of oxide are found as well as regions of intermittent external scale formation. Lamellar carbides are also evident. The denuded zone, as well as the smaller volume fraction of carbides near the boundary of this zone, indicates that the more stable internal oxides form at the expense of the internal carbides. The carbides are being dissolved rather than directly oxidized. The Fe-24.4 Cr alloy of Figure 14 formed an external oxide scale, but carburization was also found in a layer beneath

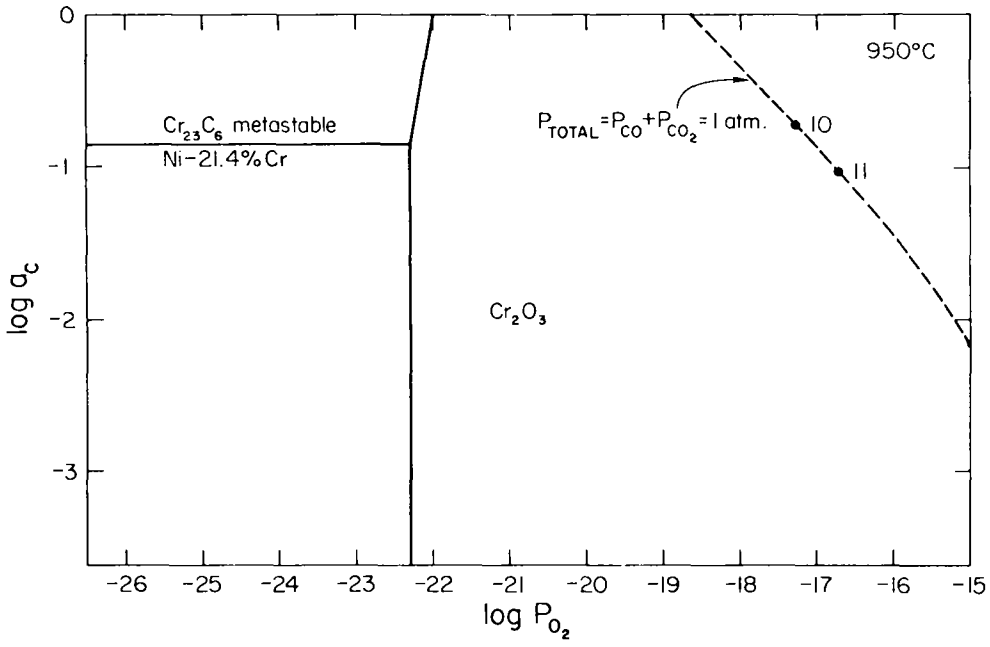

Fig. 8—Ni-Cr-C-O metastability plot at 950 °C.

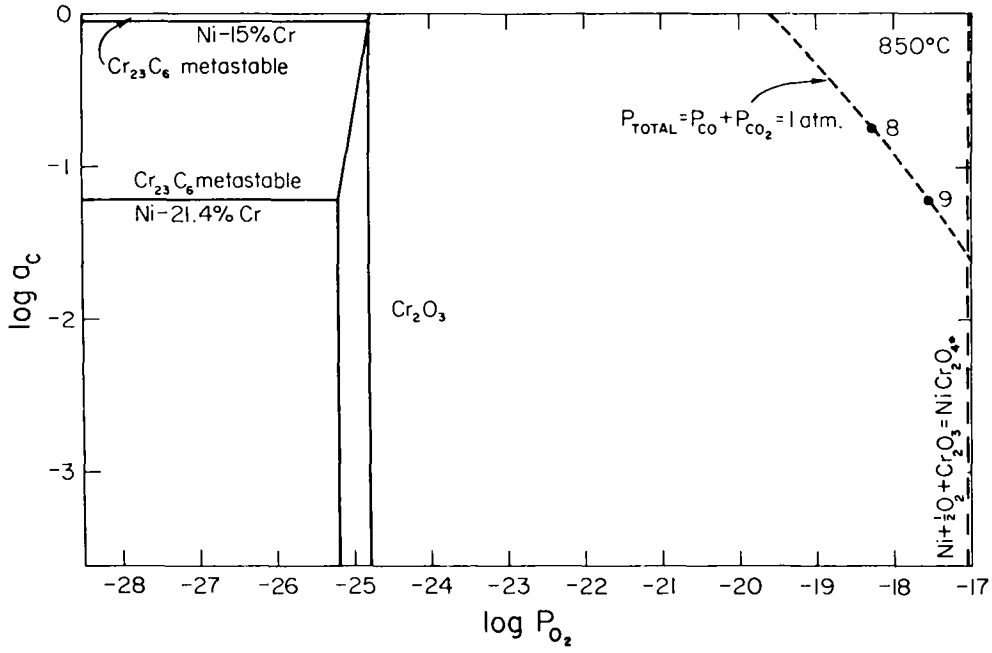

Fig. 9—Ni-Cr-C-O metastability plot at 850 °C.

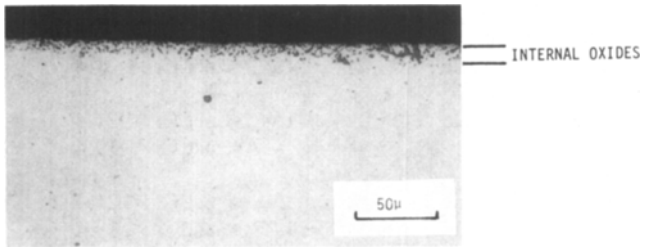

Fig. 10—Optical micrograph of the cross-section of an Fe-4.9 wt pct Cr alloy reacted at 950 °C with P_{CO_2}/P_{CO} = 0.11 for 12 h. Etched but no carbides revealed.

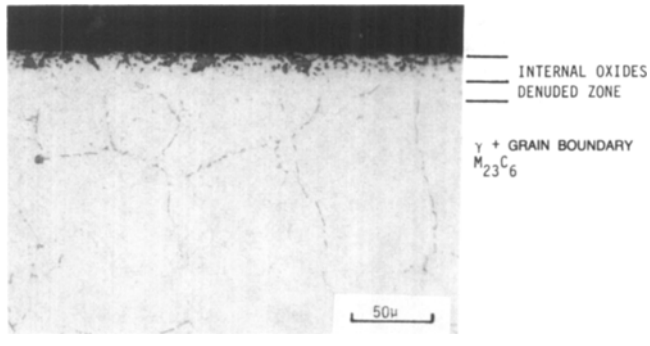

Fig. 11—Optical micrograph of the cross-section of an Fe-9.9 wt pct Cr alloy reacted at 950 °C with P_{CO_2}/P_{CO} = 0.11 for 12 h. Etched to reveal carbides.

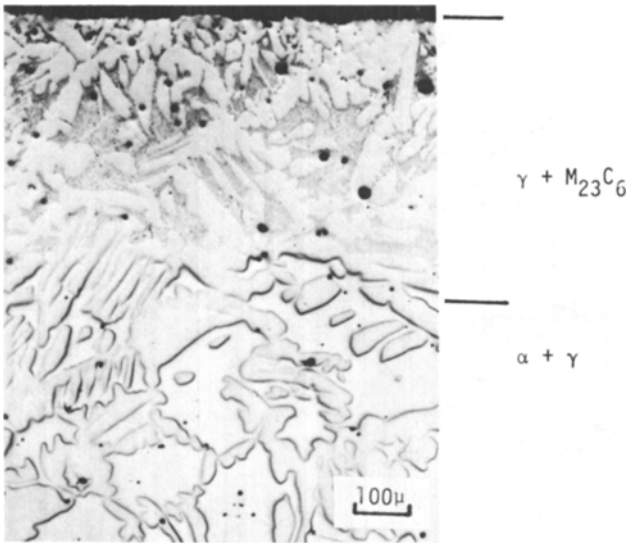

Fig. 12—Optical micrograph of the cross-section of an Fe-14.7 wt pct Cr alloy reacted at 950 °C with P_{CO_2}/P_{CO} = 0.11 for 12 h. Etched to reveal carbides.

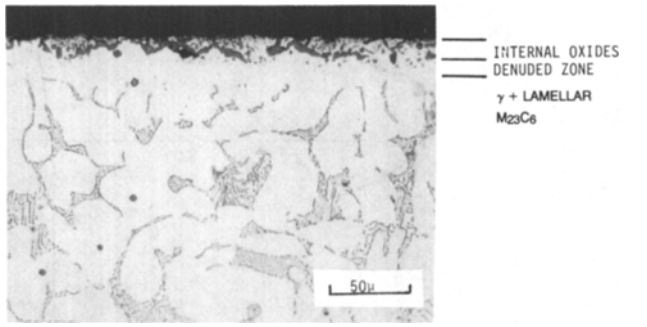

Fig. 13—Optical micrograph of the cross-section of an Fe-14.7 wt pct Cr alloy reacted at 950 °C with P_{CO_2}/P_{CO} = 0.11 for 12 h. Etched to reveal carbides.

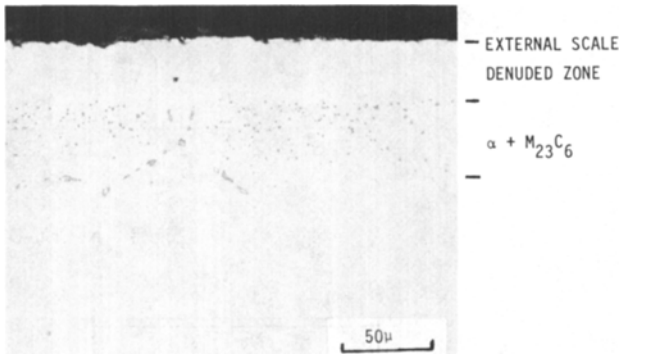

Fig. 14—Optical micrograph of the cross-section of an Fe-24.4 wt pct Cr alloy reacted at 950 °C with P_{CO_2}/P_{CO} = 0.11 for 12 h. Etched to reveal carbides.

the scale. General precipitation of carbides within grains and grain boundary precipitation was observed. Internal carbides have also been observed beneath Cr_2O_3 scales on FeNiCr alloys exposed to oxidizing and carburizing atmospheres.[10,11] Thus, Cr_2O_3 scales are not perfect barriers to carbon penetration. Wolf and Grabke[12] showed by radiocarbon measurements that Cr_2O_3 and several other oxides exhibit no detectable carbon solubilities in the lattice or at grain boundaries. Thus, carbon penetration through Cr_2O_3 can occur only by transport of carbon-bearing molecules through pores and cracks in the oxide. Alternatively, carbides could form during the initial transient stages of oxidation prior to the stabilization of the external Cr_2O_3 scale.

Table III summarizes the optical metallography results and the carburization predictions from the metastability plots (Figures 6 through 9). Table III also shows where the transition from internal oxidation to external scaling occurred for each experiment. For example, in experiment 2, the transition occurred between Fe-14.7 and 19.4 wt pct Cr, and in experiment 8 between Ni-15 and 21.4 wt pct Cr. In Table III, the predictions for carburization by $M_{23}C_6$ formation are reasonably close to the experimental observations. This is in view of the fact that the stability diagrams were constructed using data for pure carbides while alloy carbides are actually formed. In experiment 2, carburization occurred in two alloys more dilute than the predicted one, a deviation in alloy composition of about 5 pct Cr. In experiment 3, the prediction for carburization changes, but again the experimental result differs from the prediction by

Table III. Comparison of Metallographic Observations with Predictions from Stability Plots (Figures 6 through 9)

Experiment	Alloy Composition Predicted for Carburization	Alloy Composition Observed to Exhibit Carburization	Minimum Alloy Composition to Form Protective Cr_2O_3 Scale
2, Fe-Cr	11.8 < pct Cr < 14.7	4.9 < pct Cr < 9.9	14.7 < pct Cr < 19.4
3, Fe-Cr	14.7 < pct Cr < 19.4	9.9 < pct Cr < 11.8	14.7 < pct Cr < 19.4
4, Fe-Cr	14.7 < pct Cr < 19.4	11.8 < pct Cr < 14.7	14.7 < pct Cr < 19.4
5, Fe-Cr	19.4 < pct Cr < 24.4	11.8 < pct Cr < 14.7	19.4 < pct Cr < 24.4
6, Fe-Cr	4.9 < pct Cr < 9.9	11.8 < pct Cr < 14.7	14.7 < pct Cr < 19.4
7, Fe-Cr	9.9 < pct Cr < 11.8	9.9 < pct Cr < 11.8	14.7 < pct Cr < 19.4
8, Ni-Cr	15 < pct Cr < 21.4	no carburization, external Cr_2O_3 scale	15 < pct Cr < 21.4
9, Ni-Cr	pct Cr ≃ 21.4	no carburization, external Cr_2O_3 scale	15 < pct Cr < 21.4
10, Fe-Cr	11.8 < pct Cr < 14.7	14.7 < pct Cr	14.7 < pct Cr < 19.4
Ni-Cr	15 < pct Cr < 21.4	no carburization, external Cr_2O_3 scale	15 < pct Cr < 21.4
11, Fe-Cr	14.7 < pct Cr < 19.4	pct Cr < 14.7	14.7 < pct Cr < 19.4
Ni-Cr	21.4 < pct Cr	no carburization, external Cr_2O_3 scale	15 < pct Cr < 21.4

two alloys. However, in this experiment the two most concentrated alloys which should have carburized did not, undoubtedly because the presence of an external oxide scale prevented carbon penetration. In experiment 4, carburization occurred in an alloy that was more dilute than the prediction, while in experiment 6 carburization occurred in the alloy that was more concentrated than the prediction. In most experiments, the difference between the prediction and experiment only amounted to a few weight percent Cr.

In the case of the Ni-Cr alloys, carburization could not be adequately evaluated because carburization was never observed in any of the alloys. Carburization of these alloys was predicted only for alloys that formed external scales, and a compact, adherent external scale is a barrier to carbon penetration.

Because of experimental limitations, the Ni-Cr alloys could not be reacted in very reducing gas mixtures. Consequently, it could not be determined at what carbon activity (greater than the thermodynamic requirement) carburization might initiate in the Ni-Cr alloys.

The important practical difference in carbide-forming tendency for Fe-Cr *vs* Ni-Cr alloys is well appreciated in alloy selection for carburizing environments. The differing carbide-forming tendencies can be explained by the lower value for the chromium activity coefficient in the Ni-Cr system compared to the Fe-Cr system and by the smaller solubility for Ni in $M_{23}C_6$ compared to Fe. One would not expect the physical barrier to carbon penetration (external scale) to be substantially different for Fe-Cr and Ni-Cr alloys, but this may play a role also.

The reasonably close prediction of "metastable" carburization was realized even though the alloy/carbide equilibria lines on the metastable diagrams were based on the assumption that pure $Cr_{23}C_6$ would form. However, the $M_{23}C_6$ carbides dissolve substantial amounts of iron so that the Gibbs energy of formation of an alloy carbide in an Fe-Cr alloy is somewhat lower than that of pure $Cr_{23}C_6$. This, in turn, lowers the carbon activity needed for the alloy-carbide equilibrium. Such a shift is in the proper direction to explain the small disparity between the predictions and observations from experiments. Another factor can cause a shift in these boundary positions. The interaction parameter of carbon upon chromium[4] is about -11 at 950 °C which will cause the activity of chromium to decrease in the presence of carbon (the magnitude depends upon the amount of carbon). Thus, dissolution of carbon from the gas into the alloy causes the stable alloy field to expand, which is opposite the shift resulting from consideration of alloy carbides rather than pure carbides. The interplay between these "second order" factors probably establishes the exact position of the alloy/carbide boundaries. Unfortunately, no Gibbs energy data are available for the $M_{23}C_6$ alloy carbides. However, predictions based on the formation of pure $Cr_{23}C_6$ without the consideration of solution effects and interaction coefficients were reasonably close to the observations.

Thus far, the discussion has considered only isothermal carburization. Alternatively, one could consider that some carbides precipitated upon cooling. Upon lowering the temperature, carburization does become thermodynamically more favorable for a given alloy and gas composition; this can be seen by reconsidering Figure 1. Thus, for alloys near the Zone I/Zone II boundary, a slow quench from temperature could result in carbide precipitation. In this particular study, the samples were cooled rapidly by raising the samples from the furnace hot zone into a cool zone outside the furnace. For this reason, the stabilization of $M_{23}C_6$ by some Fe dissolution is considered more important in shifting zone boundaries than any slowness in quenching.

In all but one case of carburization, a denuded zone was found between the oxide (as internal precipitates or as a scale) and the carbides. The denuded zone indicates that the carbides are dissolved rather than oxidized. However, in experiment 5, the Fe-19.4Cr alloy formed lamellar carbides and internal oxides with the absence of a denuded zone; this indicates that the carbides were directly converted to oxides. The denuded zones may be explained by concentration gradients and thermodynamic interaction effects. Because carbon lowers the activity of chromium, a carbon concentration gradient implies an opposite chromium activity gradient even if there is no chromium depletion. When chromium depletion is also present the effect is more pronounced. Figure 15 shows the two generally observed corrosion morphologies: A, internal oxidation with carburization and B, external scaling with carburization. Also in Figure 15, a schematic isothermal phase stability diagram is shown which proposes corresponding reaction paths. Because the presence of carbon decreases the chromium activity[5] near the surface of the alloy where the carbon activity is high, the chromium activity is lower than inside the alloy where the carbon activity is low. Likewise, chromium depletion at the alloy surface decreases the chromium activity further, in addition to the carbon effect. On the diagram a_C' represents the carbon activity in the gas at the external surface and a_C'' represents the carbon activity inside the alloy, where carbon has a negligible effect on the chromium activity. Since a carbon gradient from the surface to the alloy interior is established for relatively short reaction times, there will be a corresponding chromium activity gradient. Thus, the alloy/carbide equilibrium will exist at various carbon activities corresponding to changing chromium activities; this implies a curved alloy/carbide boundary as position in the alloy changes. Schematic reaction paths for cases A and B have been constructed to show how the denuded zones can be explained by the carbon and chromium gradients and interactions in the alloy which accomplish a local destabilization of the carbide. The numbers on the reaction paths correspond to the numbers on the schematic cross-sections. These depict important positions in the alloy such as the scale/alloy interface and internal carburization boundaries.

From previous work on noble metal-alloy oxidation,[11] the concentration of the protective component required to accomplish the transition from internal oxidation to the formation of an external protective scale is expected to decrease as the oxygen activity decreases. However, in the current investigation, the entire range of oxygen activities was restricted to a variation of less than two orders of magnitude. Thus, no large shift in the "transition" chromium content was observed for either the Fe-Cr or Ni-Cr systems. In all runs but one (#5), the Fe-19.4 Cr alloy formed an external Cr_2O_3 scale; in each experimental run, the Ni-21.4Cr alloy formed an external Cr_2O_3 scale.

V. SUMMARY AND CONCLUSIONS

A method for predicting the onset of "metastable" carburization based upon thermodynamic metastability diagrams

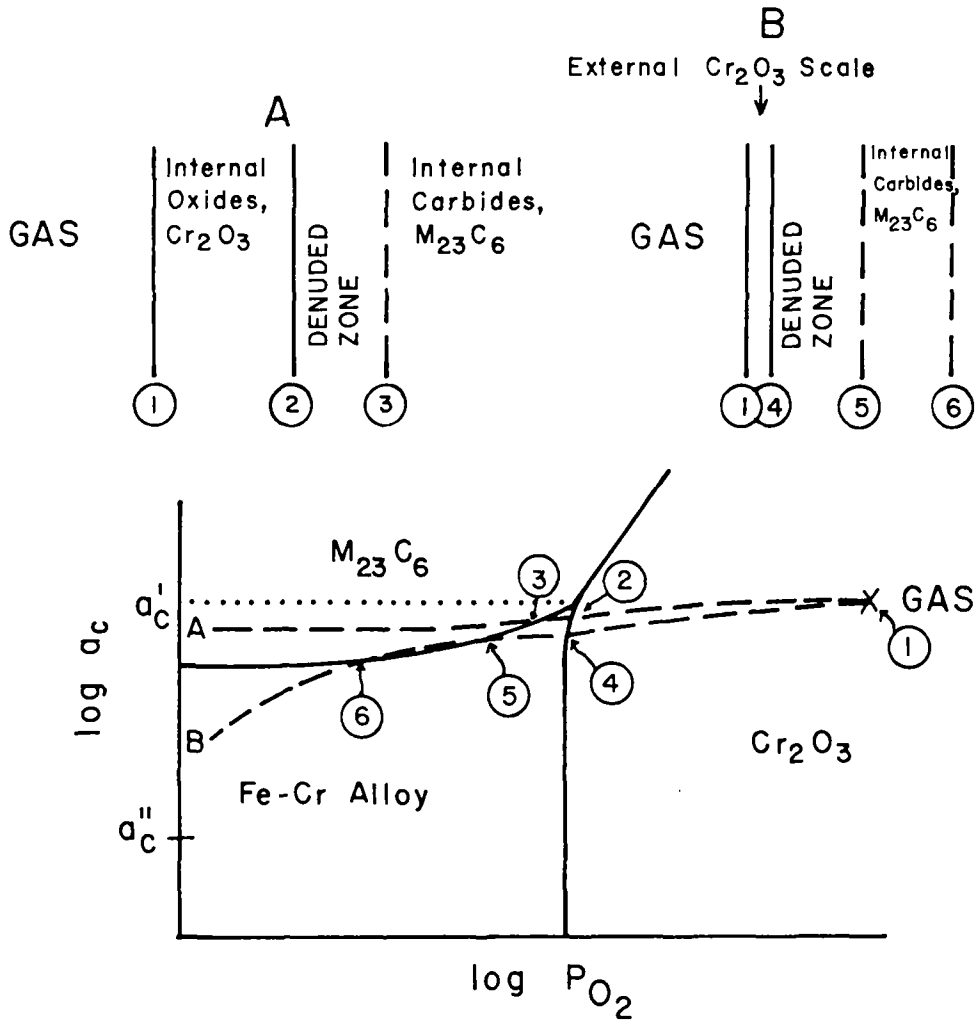

Fig. 15 — Schematic reaction paths plotted on a metastable diagram for both external scale formation and internal oxidation. The interaction of carbon on chromium activity and a chromium depletion is considered to explain denuded zones.

was developed and tested experimentally. The predictions are reasonably close to the experimental observations. Thus, the formation within an alloy of a compound that is not stable in the alloy in contact with the gas phase is understandable on the basis of a thermodynamic argument. More accurate thermodynamic data are necessary to develop a more quantitative model. Little carburization was seen in alloys that formed external Cr_2O_3 scales on Fe-Cr alloys, and these precipitates may have formed during an initial transition period prior to the establishment of the protective scale. No carburization was observed in the Ni-Cr alloys, but the only alloys that were predicted to carburize were the ones that formed external scales. Thus, a Cr_2O_3 scale acts as an effective barrier to carbon penetration for short times (12 hours). The clearly different tendencies of Fe-Cr and Ni-Cr alloys for carburization can also be understood in terms of a marginally lower thermodynamic stability of $M_{23}C_6$ in the Ni-Cr alloys.

ACKNOWLEDGMENTS

This research was supported by the Electric Power Research Institute under contract RP716-2, R. Jaffee and J. Stringer, Project Managers.

REFERENCES

1. B. E. Hopkinson and H. R. Copson: *Corrosion*, 1960, vol. 16, p. 608t.
2. F. S. Pettit, J. A. Goebel, and G. W. Goward: *Corr. Sci.*, 1969, vol. 9, p. 903.
3. A. D. Kulkarni and W. L. Worrell: *Metall. Trans.*, 1972, vol. 3, p. 2363.
4. F. N. Mazandarany and R. D. Pehlke: *Metall. Trans.*, 1973, vol. 4, p. 2067.
5. T. Wada, H. Wada, J. Elliott, and J. Chipman: *Metall. Trans.*, 1972, vol. 3, p. 2865.
6. R. Perkins: Lockheed Space and Missile, Inc., Palo Alto, CA.
7. L. R. Woodyatt and G. Krauss: *Metall. Trans. A*, 1976, vol. 7A, p. 983.
8. K. Bungardt, E. Kunze, and E. Horn: *Arch. Eisenhüttenwes.*, 1958, vol. 29, p. 193.
9. C. T. Fujii and R. A. Meussner: *J. Electrochem. Soc.*, 1967, vol. 114, p. 435.
10. A. Schnaas and H. J. Grabke: *Oxid. Metals*, 1978, vol. 12, p. 387.
11. H. J. Grabke, K. Ohla, J. Peters, and I. Wolf: *Werkstoffe und Korrosion*, 1983, vol. 34, p. 495.
12. I. Wolf and H. J. Grabke: *Solid State Comm.*, 1985, vol. 54, p. 5.
13. R. A. Rapp: *Acta Metall.*, 1961, vol. 9, p. 730.